In-Situ Transmission Electron Microscopy Observation of Germanium Growth on Freestanding Graphene: Unfolding Mechanism of 3D Crystal Growth During Van der Waals Epitaxy

Thierno Mamoudou Diallo, Mohammad Reza Aziziyan, Roxana Arvinte, Jean-Christophe Harmand, Gilles Patriarche, Charles Renard, Simon Fafard, Richard Arès, Abderraouf Boucherif

In-situ transmission electron microscopy observation of germanium growth on freestanding graphene: Unfolding mechanism of 3D crystal growth during Van der Waals epitaxy

Thierno Mamoudou Diallo[1,2], Mohammad Reza Aziziyan[1,2], Roxana Arvinte[1,2], Jean-Christophe Harmand[3], Gilles Patriarche[3], Charles Renard[3], Simon Fafard[1,2], Richard Arès[1,2*], Abderraouf Boucherif[1,2*]*

[1]Institut Interdisciplinaire d′Innovation Technologique (3IT), Université de Sherbrooke, 3000 Boulevard Université, Sherbrooke, J1K OA5 Québec, Canada.

[2]Laboratoire Nanotechnologies Nanosystèmes (LN2)-CNRS UMI-3463 Institut Interdisciplinaire d′Innovation Technologique (3IT), Université de Sherbrooke, 3000 Boulevard Université, Sherbrooke, J1K OA5 Québec, Canada.

[3]Université Paris-Saclay, CNRS, Centre de Nanosciences et de Nanotechnologies (C2N), 91120 Palaiseau, France

*Correspondence to: Thierno.mamoudou.diallo@usherbrooke.ca, Richard.ares@usherbrooke.ca, Abderraouf.boucherif@uhserbrooke.ca

Keywords: in situ TEM, graphene, Van der Waals epitaxy, vertical diffusion, Ostwald ripening

Breakthrough in cutting-edge research fields such as hetero-integration of materials and development of quantum devices is heavily bound to the control of misfit strain during heteroepitaxy. While remote epitaxy offers one of the most intriguing avenues, demonstrations of functional hybrid heterostructures is hardly possible without deep understanding of the nucleation and growth kinetics of 3D crystals on graphene and their mutual interactions. Here, we unravel kinetics of such processes from real-time observations of germanium (Ge) growth on freestanding single layer graphene using in-situ transmission electron microscopy. This powerful technique provides a unique opportunity to observe new and yet unexplored phenomena, which were not accessible to the standard ex situ characterizations. Through direct observations, we elucidate remote interactions between Ge crystals through the graphene layer in double heterostructures of Ge/graphene/Ge. Notably, our data show real-time evidence of vertical Ge atoms diffusion through the graphene layer. This phenomenon is attributed to the remote interactions of Ge atoms through the graphene lattice, due to its interatomic interaction transparency. Additionally, key mechanisms governing nucleation and initial growth on graphene were systematically determined. These findings enlighten the growth mechanism on graphene and provide a new pathway for disruptive hybrid semiconductor-graphene devices.

1. Introduction

Van der Waals (VdW) heterostructures, including two-dimensional (2D) layered materials and conventional three-dimensional (3D) materials with surface dangling bonds, have ignited a great deal of interest because of the unique functionalities arising from such an integration.[1],[2] Due to the VdW interactions, diverse practical devices were attempted, such as heterojunction electronics,[3],[4],[5] mechanically transferrable optoelectronics,[6],[7] and biomolecular electronic devices.[8] Among the various materials for these applications, graphene provides an ideal model for VdW attractions, since its honeycomb structure (sp^2 hybridization) has no permanent polarity or surface dangling bonds.[9] However, while fabrication of the heterostructures of 2D material on 3D material (2D/3D) by transfer or Van der Waals epitaxy (VdWE)[1] has been well established, the epitaxial growth of single crystalline 3D on 2D heterostructures has been challenging. This is mainly due to the dissimilar chemical bonding and structure across the interfaces between 3D and 2D materials [1],[10] as well as the low surface energy of 2D materials[11]. Some of these challenges were highlighted during the growth of GaAs, InP, silicon (Si) and Ge on graphene.[11],[12],[13] More recently, atomic interactions across a graphene monolayer (1ML) has been demonstrated using the so-called remote epitaxy , where large areas of GaAs single-crystalline layers were epitaxially grown on 1ML graphene-coated GaAs wafers.[14] More recently, the remote epitaxy has been proven to be applicable to grow perfect single-crystalline films of various compound materials on graphene coated substrates.[15],[16] Such a discovery provided a significant step towards advancing the field of VdWE of 3D/2D materials. However, despite outstanding achievements and progress in understanding of the underlying mechanisms governing such remote epitaxial effects, a more descriptive understanding of nucleation and growth mechanisms is still required for obtaining perfectly planar layers through this technique. Such an achievement would enable a wider deployment of VdW heterostructures in cutting-edge technologies. Therefore, studying the nucleation and growth mechanisms, such as how nuclei are formed, how they evolve in nanomaterials and interact with the underlying substrate are but a few of the most interesting current topics in materials science. [17] For this reason, we have identified high-resolution transmission electron microscopy (HRTEM), which provides real-space images as well as atomic-resolution information on the nucleation and early stage growth, as a probe for such atomistic phenomena.

In this study, we report some indispensable details on nucleation, growth mechanisms, and interatomic interactions governing VdWE on single layer graphene (SLG). The rigorous interpretations were made from real-time observations of the nucleation and initial growth of germanium (Ge) on suspended single layer graphene (S-SLG) by using a TEM. The direct TEM observations allowed strict and meticulous examination of the nucleation and the initial behavior, thereby unfolding their kinetics. We also report direct experimental observation of the Ostwald ripening process, which governs the coarsening of the Ge particles on S-SLG. Furthermore, the crystalline structure of the Ge crystals was also investigated. Most importantly, due to the remote interatomic interactions, our work demonstrated the possibility of vertical Ge diffusion through the SLG from Ge/S-SLG/Ge double heterostructures. Such heterostructures are formed because of the use of S-SLG and ultra-high vacuum chemical vapor deposition (UHV-CVD), since in such a configuration, Ge nuclei are growing from both sides of the SLG. These findings provide invaluable information about remote interatomic interactions as well as the nucleation and growth processes, from real-time TEM observation, a unique vantage point that sheds light on the dynamical aspects of such atomic-scale events.

2. Results and discussions

2.1. Nucleation of Ge on S-SLG

Figure 1 illustrates the analysis of the in situ TEM observation of Ge growth on a suspended single layer graphene during nucleation and at early stages of growth process.

Prior to the in-situ growth observation, the experiment started with fabrication of the freestanding single layer graphene (Figure 1a) on E-chips (heating membranes). The details on the graphene transfer and the sample preparation are given in the methods section. Ge crystals nucleate on the clean graphene by heating the samples, at different temperatures, and exposing them to a flux of digermane gas (Ge_2H_6), as shown in Figure 1a. We assumed that the system was under a “supersaturation regime” and the Ge adatoms on the graphene surface were moving through a standard surface diffusion process. When Ge adatoms encounter each other, there is a chance that they form a bond (covalent), which produces a nucleus. As it grows, the nucleus is constituted of internal atoms (hatched red circles) and periphery atoms (blue) (Figure 1b). According to the thermodynamics of nucleation, the total Gibbs free energy of a system depends on the chemical bonds that are part of the system. Therefore, as a primitive perception, it is less probable that an internal atom leaves the germ (breaking six bonds and creating six dangling bonds), while a periphery atom can leave more easily,

because it must break fewer bonds to do so. In the same way, new adatoms are constantly impinging on the germ periphery from the vapor phase. If the rate of uptake of adatoms at the germ's periphery surpasses the rate of escape, the germ grows.

Figure 1a shows a TEM image of Ge germs during the nucleation process. This nucleation was obtained at a growth temperature as low as 220 °C. However, regardless the growth temperature, we noticed that the nucleation maintains a Frank and Van der Merwe (FM) growth mode, by opposition with the Stranski-Krastanov (3D growth) that is observed in large mismatch material systems. Since the lattice mismatch between the two materials is very large, the FM mode confirms that there are likely few, if any, covalent bonds between the Ge layer and the underlying graphene, confirming the VdW bonding nature of our system.[18] The weak bond strength, typical of VdW, favors the elastic relaxation of the Ge germs. At growth temperatures higher than 220 °C, we found that the nucleation on the clean graphene is much more challenging due to the low surface energy of the graphene and the high diffusion length of the adatoms at those temperatures. Therefore, for nucleating on the suspended single layer graphene, our strategy was to use two-step nucleation: nucleating at low temperatures due to the decreased diffusion length and the increased adsorption, following by annealing the resultant germs to improve the crystalline quality. As a result, circular germs with an average area from 1.5 to 2 nm^2 were obtained (Figure 1c). We can also notice that particle growth and nucleation occurred in parallel (see germs highlighted by arrows in Figure 1a, showing examples of early-stage growth).

From the growth video (movie S1), we can see that germs are formed and desorbed until they reach a stable size, enabling the energetically favorable nucleation. This is illustrated in the Figure 1c, showing the size of Ge particle that allowed a viable nucleation. It provides clear evidence that for the nucleation to occur, size of germs should surpass a critical value. Such a critical size corresponds to the minimum size at which a particle can survive and grow without desorption.[19],[20] Therefore, germs with a size less than the critical value are not stable, and the free energy of the system is decreased by their dissolution (movie S1). Similarly, germs with a size above the critical value are energetically stable and their growth decreases the free energy of the system. Based on Figure 1c, the critical size is determined to be between 0.7 and 1 nm^2. These sizes are comparable to those predicted by the classical nucleation theory (CNT). However, due to the very short lifetime of subcritical germs (in the order of ns) and the limited temporal resolution of the employed TEM system, it is difficult to observe germs with sizes below the critical size. Therefore, even though the sizes are similar,

we cannot confirm with certainty that the critical size found in this work is the one predicted by the CNT.

During the entire process, most of the Ge particles are circular as shown in Figure 1d. This is explained by the isotropic nature of the Ge nuclei and the high surface tension at the interface between the graphene and the Ge particles due to the lack of dangling bonds, which result in the system energy minimization. The optimized circular form leads to the assumption that there is an extreme mobility along the germ's periphery since the Ge particles and the underlying graphene are only attracted by VdW forces. In fact, during the Ge growth on graphene, Ge dimers do not form chemical bonds with the graphene, because the VdW gap (2.56 to 2.59 Å) formed between the Ge and the graphene is much longer than the Ge-C bond length (1.95 Å).[21] Therefore, the Ge germs are floating at the top of the underlying graphene substrate, making the atom's diffusion at the peripheries very high.

Along with the conventional crystalline growth by means of adatoms from the vapor phase, frequent particle coarsening events could occur during the nucleation process. Figure 1e shows the density of visible particles as a function of time. At the early stage of growth, number of visible germs gradually increased and reached a first maximum around 100 s. During the coarsening, however, the density of the particles significantly decreased and reached a minimum at around 120 s. Later, a second increase in the number of particles, due to new nucleation events, was observed, which continued up to 150 s. Finally, after 150 s, the number of particles drastically dropped and eventually fixed at a constant value. As observed in the growth videos, decrease of the particle density was mainly due to the coarsening events between individual germs. Therefore, when nucleation dominates the coarsening, the number of particles increases; otherwise, it decreases. In the static regime, either there was no new nucleation and coarsening event or the number of events for the two processes became similar.

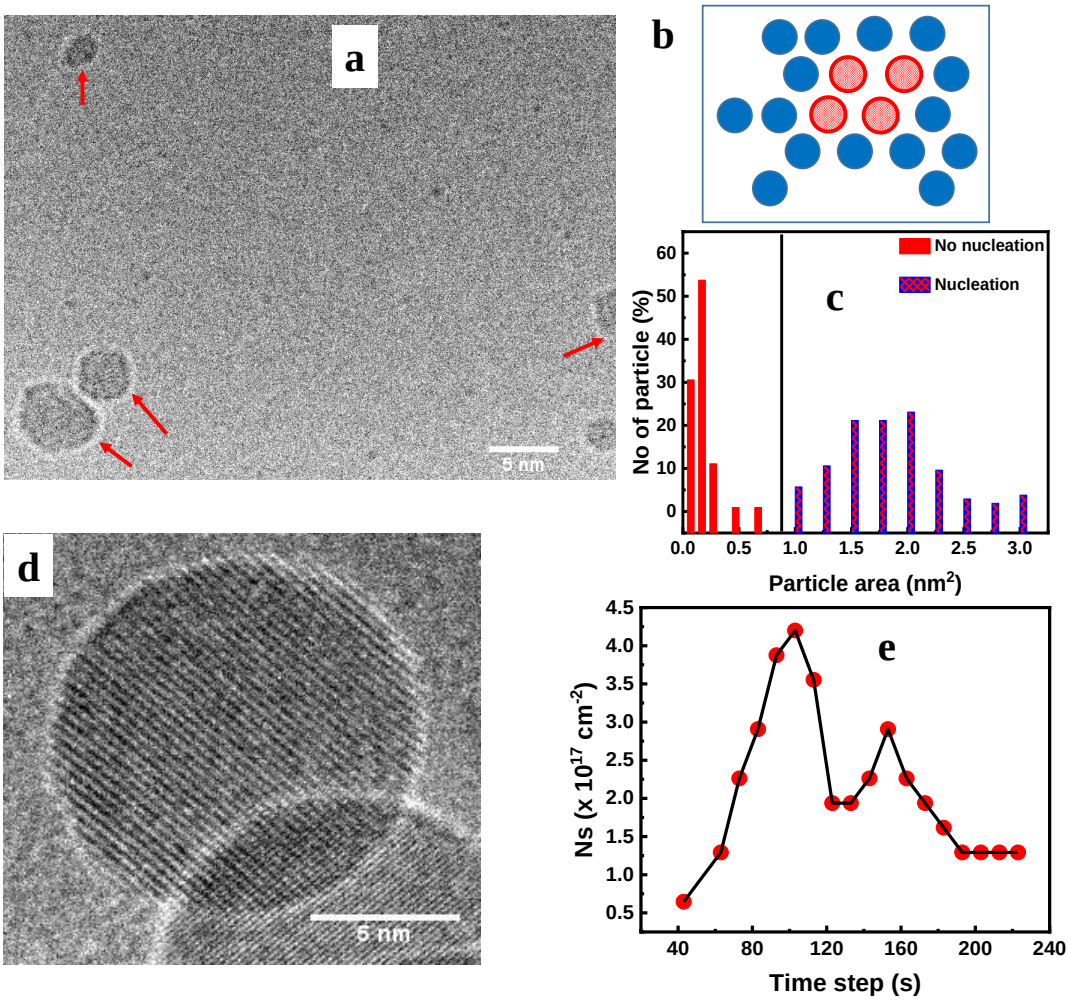

Figure 1. Analysis of in situ TEM growth of Ge on suspended single layer graphene (S-SLG). (a) TEM image of germs during the nucleation process. Some germs are growing while others are still nucleating (see red arrows). (b) Schematic illustration of different types of atoms in a germ. Blue circles are periphery atoms with dangling bonds and hatched red ones are surface atoms (c) Particle area distribution showing the limit size enabling the nucleation of Ge on the S-SLG. (d) High-resolution TEM image of a Ge crystal during the growth process. (e) Number of visible particles versus time steps. The germ areas were determined from HRTEM growth videos.

2.2.Nucleation and growth kinetics

To analyze Ge growth on the S-SLG and determine the mechanisms governing the growth process, we followed the lateral expansion of Ge germs in real-time videos recorded during the in situ TEM observation of the growth. The analysis of data is presented in **Figure 2**. The sequence of HRTEM images of the nucleation and the early stage growth of germs, grown at 350°C, are illustrated in Figure 2a. At 350 °C, the first stable germ nucleated after approximately 44 s. Note that the mobility of the digermane molecules is very high on the surface and therefore, they will move very fast once they reach the graphene surface. Through a thermodynamic process, those molecules will be dissociated once they encounter an energetically favorable site (dangling bonds, imperfections, etc.). Following their dissociation

on an energetically favorable site of the graphene surface, the concentration of the active Ge species increases until it reaches a critical supersaturation level that allows the nucleation of a stable Ge germ to take place. This means that at the very early stages until a critical germ is obtained, the nucleation mechanism could be controlled by the digermane dissociation on the graphene surface. With our experimental data, we observed that in the range of the studied temperatures, the dissociation of the precursor (Ge_2H_6) directly on the substrate appeared to be relatively fast. In addition, once stable germs are obtained, it is expected that the digermane molecules dissociate on those germs and their peripheries (atomic step at the interface with the SLG) because these regions should be more reactive than the SLG surface and eventually the thermal barrier is lower. However, the growth movies showed clear evidence that germs are preferentially growing in the lateral direction allowing us to say that atoms are attaching at the peripheries of the stable germs. This means that actives species are diffusing toward the peripheries regardless their dissociation site. It is worth mentioning that in some cases we observed Ge nucleation to be faster/preferential within the e-beam exposed area. This could be mainly due to electron-beam induced digermane cracking (dissociation)[14], which increases the Ge supersaturation. However, we think those observed effects of the e-beam do not affect the general validity of the growth phenomena or induce damage and modification of the graphene layer. In fact, we observed that the graphene is damaged only in the case of a highly focused e-beam, which was not the case during the experiments. Following the initial nucleation, As shown in this figure 2a, the Ge germs show a continuous increase of size and maintain a very optimized circular shape during the early stage growth. The circular shape is maintained even after a coalescence event of the particles. These germs are crystalline and the uniform contrast within the whole germ indicates that the germs are made of single layers.

To determine and understand the growth kinetics, we extracted the lateral growth rate (dA/dt) as a function of the area (A) of the germs from image sequences such as Figure 2a. The results of the analysis are presented in Figure 2b. We supposed that the nucleation and the growth processes of the Ge crystals are treated by consideration of the atomic processes such as adatom capture, surface diffusion and re-evaporation.

During the VdWE, particularly in the case of Ge on graphene, the surface diffusion barrier is significantly decreased by the VdW bonds,[11] resulting in a large diffusion coefficient for adatoms. This means that there is a high probability for an adatom to find an existing stable germ, before another adatom is deposited in its vicinity to enable nucleation.

Consequently, the growth process on graphene is more likely to be limited by the adatom attachment rate at the peripheries of existing nuclei that are larger than the critical size.

Our simple kinetic model, based on the framework of Robinson and Robins model,[22] assumes that Ge germs nucleate with a circular shape at a critical size and the nucleation arises from the crystallization of a supersaturated fraction of Ge adatoms. Therefore, we could reckon that the growth rate of Ge nuclei is the difference (competition) between the Ge adatoms attaching to the nucleus peripheries and those leaving:

$$\frac{dA}{dt} = k_a C_{gr}\sqrt{A} - k_e\sqrt{A}, \qquad (1)$$

where *A* is the nucleus area, C_{gr} is the concentration of Ge adatoms on the graphene surface, k_a and k_e are constants that define the equilibrium concentration of Ge adatoms. From equation (1), the rate of atoms arriving ($k_a C_{gr}\sqrt{A}$) is proportional to C_{gr} and to the perimeter of the Ge nucleus ($A^{1/2}$), and $k_e A^{1/2}$ is the rate of atoms desorbing from the nucleus.

In the Figure 2b, the graphs are well fitted to the equation (1), in which the growth rate does not tend to zero for $A \rightarrow 0$. The finite intercept is because at an area below the critical size, the growth rate becomes negative since the subcritical nucleus is evaporating. This signifies that at the beginning of the nucleation process following the dissociation of the Ge_2H_6 molecules, the Ge atoms are primarily adsorbed on the graphene surface. The fitting of the graphs in Figure 2b supports that the growth of Ge on S-SLG is controlled by the Ge adatom attachment rate at the nuclei peripheries. Note that for the growth at 350 °C, in addition to the equation (1), there is a contribution from a linear dependence with the surface area. Therefore, in that case the graph is fitted by $dA/dt = k_a C_{gr}\sqrt{A} - k_e\sqrt{A} + A$. This linear aspect reveals that the Ge germs also grow by adsorption of the digermane from the vapor phase directly onto the peripheries of the existing nuclei. A similar observation was previously reported during the SnS growth on graphene layers.[23] The same growth mechanism was observed for the different explored growth temperatures (Figure 2b). Figure 2c showing the lateral growth rate as a function of area for three selected particles (P1, P2 and P3), as examples, at 400 °C provides a further evidence of the growth mechanism. However, for identical flux of digermane during the CVD growth, the lateral growth rate increased considerably fast with the area of the germs at the lower growth temperature (Figure 2b), suggesting that the adatom evaporation part of the growth process plays an important role. As the temperature is lowered, the germ grows faster, because it loses fewer atoms to evaporation, which is competing with the growth process. This is in good agreement with the Robinson

and Robins theory,[22] which states that at low temperatures the density of adatoms is controlled primarily by the rate at which adatoms are captured by the growing nuclei, thus the rate of re-evaporation is negligible.

We also analyzed the evolution of the particle area as a function of growth time to determine the kinetics of the coalescence process. The particle size as a function of growth time at different growth temperatures (350, 400 and 600°C) is shown in Figure 2d and 2e. Here, the effective particle size of $D = 2 \times \sqrt{A}/\pi$ was used, wherein A is the area of the germ extracted from the growth videos. For time lapse after 75 s (Figure 2e), not shown in the figure, we observed that particles resulting from coarsening events exhibit a jump of particle area (see Figure S3b) following each coarsening event. A similar observation was reported during the growth of platinum nanocrystals.[24] In fact, stable germs were growing through multiple coarsening events, which minimized the total free energy of the system by forming bigger germs.

During the crystal growth, the coarsening of the particles can be described by the Ostwald ripening (OR) process, which involves the growth of larger particles at the expanse of the smaller ones. The OR is due to the difference in chemical potential that arises from the difference in the radius of curvature of the particles. This process is described by the classical kinetic model of Lifshitz-Slyozov-Wagner (LSW).[25],[26] The general kinetic equation for the OR is defined by equation (2), where D and D_0 are the mean particle sizes at time t and t_0 (time at which the germ reaches the critical size and becomes stable), k_{OR} is a material constant that depend on temperature, and n is an exponent relevant to the coarsening mechanism.

$$D - D_0 = k_{OR}(t - t_0)^{1/n}, \qquad (2)$$

From equation (2), it can be noticed that the particle size increases regularly with the increase of the time. The mechanism controlling the OR process is determined by the exponent n values. For a physical meaning, n should have values from 1 to 5. When n = 1, the growth is linear and is controlled by the attachment-detachment reactions at the peripheries;[27] when n = 2, the ripening is purely attachment limited;[28] when n = 3, the growth is purely controlled by the volume diffusion (infinite attachment rate at the germ's boundaries);[28] when n = 4, the growth is controlled by the dissolution kinetics at the particle-substrate interface.[26],[29]

Given the relation between the size (D) and the area (A) of particles, the evolution of the particle area versus time will be as follows: $A\sim t\hat{}(2/n)$. In our experiments, curves in the Figure 2d and 2e are well fitted by a combination of two equations in the form of equation (2). We found that the best fit is obtained when $n = 1$ and $n = 2$. Therefore, the fitting equation in the case of $t_0 = 0$ is in the form given by equation (3), where A_0 is the starting size, B and C are constants:

$$A = A_0 + Bt + Ct^2, \quad (3)$$

$n = 1$ and $n = 2$ suggest that the kinetics of the OR process are governed by the rate of attachment-detachment process at the germ boundaries i.e., attachment-limited regime. In this regime, the attachment and the detachment at the germ boundaries are slow compared to the diffusion of adatoms on the surface of the layered material. Similar growth kinetics were observed for different temperatures (350, 400 and 600 °C) (Figure 2d) and for different germs at the same temperature (Figure 2e). This is consistent with the growth mechanism determined in Figure 2b and 2c. The fitting parameters are summarized in the table S1 of the supplementary materials.

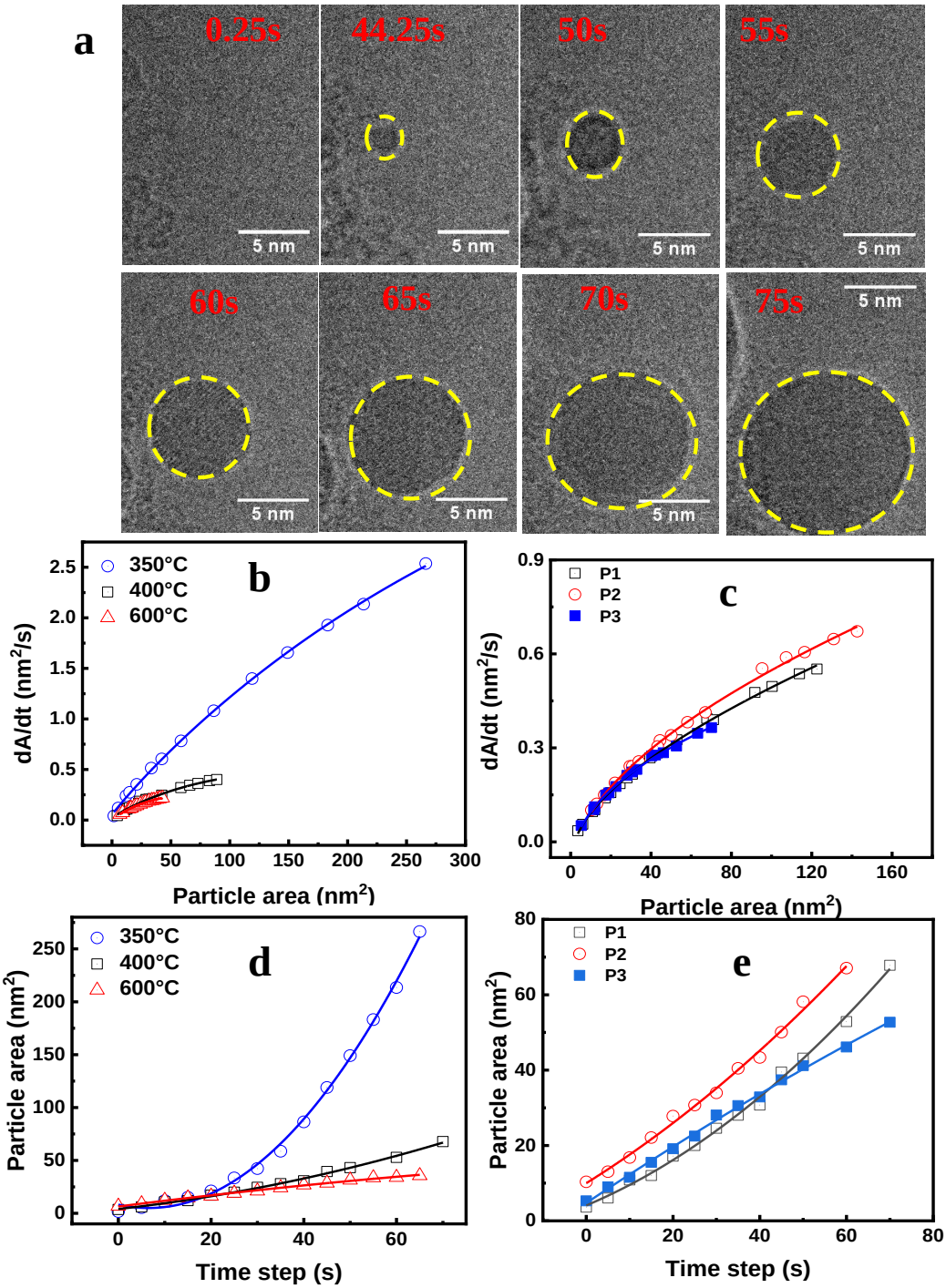

Figure 2. Analysis of the kinetics of Ge growth on S-SLG from real-time TEM observations: (a) HRTEM image sequence showing the nucleation and initial growth of a single Ge germ on S-SLG at Tg=350°C. (b) Analysis of the Ge lateral growth rate (dA/dt) as a function of the particle area, A, at 350, 400 and 600 °C. (c) lateral growth (dA/dt) as a function of the particle area (A) for 3 different particles at 400 °C. (d) Particle area versus elapsed time from the initial nucleation presented in (b). (e) Area as a function of elapsed time for the 3 particles presented in (c). The particle areas were measured from the growth videos. All analyzed nuclei showed the same general growth behavior.

2.3.Crystalline structure and epitaxial relationship of Ge crystals

Figure 3 illustrates Ge crystals and their crystalline structure during the real-time studies of Ge growth on freestanding single layer graphene. Figure 3a and 3c show the

HRTEM images of Ge crystals grown at two different temperatures, 350 and 600 °C, respectively. From these images, we notice that Ge germs are crystalline and defect-free. In the range of studied growth parameters, we found that Ge crystals are diamond cubic (DC). However, depending on the growth temperature, we observed different crystalline orientations. At 350 °C, the DC Ge crystals are mainly formed by the family of (220) planes, which have a zone axis of [111]. In this case, the epitaxial relation of the interface between the DC Ge crystal and the underlying SLG is in the form <111> Ge ‖ <0001> Gr. At such a growth temperature, 60% (3 out of 5) of the crystals follow <111> Ge ‖ <0001> Gr epitaxial relationship. It is worth mentioning that in the (111) plane of the cubic semiconductor, the atoms have a hexagonal symmetry like the carbon atoms in graphene. This is evident from the Fast Fourier Transform (FFT) pattern in Figure 3b, which is the FFT of the Ge crystal presented in Figure 3a. In Figure 3b, the Ge atoms are almost aligned with those of C in the graphene layer. At 600 °C, Ge crystals are still DC, but with another crystalline orientation ([220]). Figure 3c and 3d show a crystal grown at 600 °C and its FFT pattern, respectively. From Figure 3d, the average d-spacing was found to be 0.361 nm, which corresponds to the theoretical d-spacing (0.366 nm) of (111) family planes. Therefore, in Figure 3d, the crystal is formed of (111) planes, which have a zone axis of [220]. In this case, the epitaxial relation of the DC Ge crystal / Gr interface is defined as follows: <220> Ge ‖ <0001> Gr. Here, about 50% (5 out of 10) of the analyzed germs follow that epitaxial relationship. In this case, the diagonals of the graphene hexagonal lattice are considered as symmetry axes for the rectangular lattice of the DC Ge crystal structure. There is a 30° angle between the DC Ge crystal and the underlying graphene layer (Figure 3d). In the latter case, the atomic arrangement of Ge atoms on graphene would result in a lattice mismatch of ~ 3.3 %.[30] The above-mentioned statistics are obtained in the case of crystals grown on the clean graphene (200 to 300 nm wide regions). However, it is worth mentioning that some PMMA residues remained on the graphene layers during the cleaning process, prior to the growth, and it significantly prevented the nucleation on the clean graphene. This is because the residues act as preferential nucleation sites resulting in polycrystalline layers with different orientations (see Figure S2d and S2e of the supplementary materials). This provides a further evidence that the major limitations during the in-situ growth on graphene are the cleaning processes and the quality of the layers, which control the nucleation process. Therefore, in order to properly study the nucleation and growth mechanisms, graphene layers should be defect-free and residue-free.

The two configurations found at 350 °C and 600°C could be assigned, respectively, to the T-site, and the B-site, which are the preferential adsorption sites of Ge on graphene. Similar theoretical and experimental results have been previously reported.[30],[31],[32],[33] More details on the adsorption sites and the schematic illustrations of the FFT patterns for each of the above-mentioned cases are presented in Figure S4 of the supplementary materials.

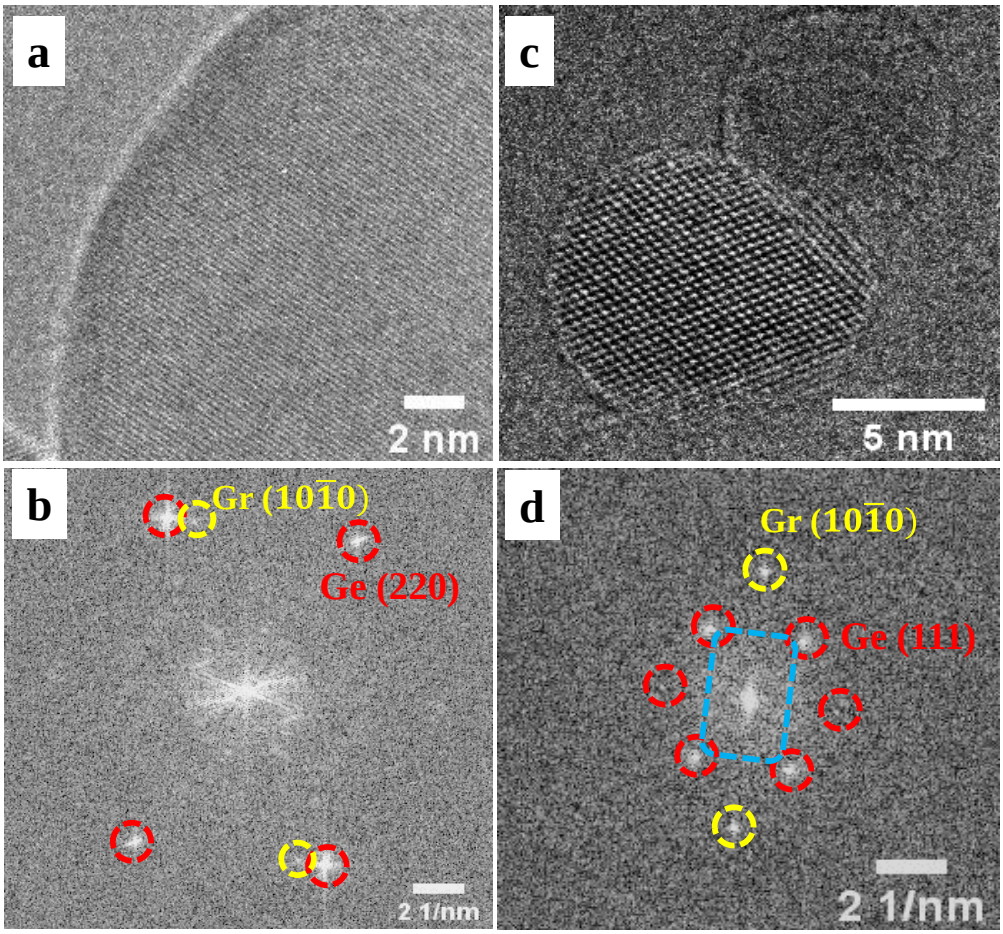

Figure 3. Crystalline structure and epitaxial relations of the Ge particles during the in-situ growth on S-SLG. (a) HRTEM of a Ge particle grown at Tg = 350 °C, showing the atomic plans, (b) FFT image of the Ge particle presented in (a) showing the relative position of Ge atoms in (220) plans with respect to the graphene layer. Those germs have an interface as follows: <111> Ge ‖ <0001> Gr. In this configuration, Ge atoms are at the top of the graphene atoms i.e., the Ge atoms are adsorbed in a T-site (top) on the single layer graphene. (c) HRTEM of a Ge germ deposited at Tg = 600 °C, showing a crystal in the zone axis, (d) FFT image of the Ge crystal presented in (c) showing (111) planes, which have a [220] zone axis. The interface is <220> Ge ‖ <0001> Gr. Here, Ge atoms (red circles) are placed on a C-C bridge (B-site) in the SLG, and the two lattices are separated by 30° angle.

2.4.Ge atom diffusion through SLG in double heterostructures Ge/S-SLG/Ge

During the in-situ growth of Ge on the S-SLG, crystals were nucleated on both sides of the suspended layer. This is because the growth was performed by UHV-CVD (vapor sources) and the single layer graphene was suspended, allowing the growth on its front and backside. Therefore, double heterostructures of Ge/S-SLG/Ge (2D/2D/2D) were formed, in

which the graphene layer is sandwiched between the two germs of Ge (**Figure 4a**). During the growth of Ge particles on both sides of the S-SLG, the precursor flow was supplied on the both sides by two diffusion pathways: through the gap above the sample holder and through the holes on the E-chips covered by the SLG. The S-SLG was transparent enough to allow examining the Ge nanostructures induced on the backside of the graphene layers. It should be noted that, if the germs are on the same side, they could not have overlap; instead, they would have coarsened either through fast ripening process (Figure S5a, movie S2) or classical coalescence (Figure S5b, movie S3) once they were at 2 nm or less distance from each other.

In the double heterostructures (Ge/S-SLG/Ge) such as the one schematically presented in Figure 4a, vertical diffusion (VD) of Ge particles through the single layer graphene has been observed. Figure 4b displays the sequence of HRTEM images showing the VD process through the single layer graphene. P1, P2 and P3 are Ge particles grown at 400 °C, wherein P1 and P3 are on the same side and P2 is on the other side of the S-SLG. From frame 1 of Figure 4b, we can see that P2 overlapped with P1 and P3; however, it did not merge. This confirms that they were not on the same side. Nonetheless, the area of particle P2 was continuously decreasing until it completely disappeared in frame 4, where the entire particle diffused through the S-SLG and merged with P3 on the other side. The size reduction of P2 is clearly illustrated in Figure 4c, showing the decreasing of the particle area as a function of frames, which were separated by 0.25s. In the Figure 4b, P1 was ripened by P3 at frame 4 (where they reach the critical distance) through a direct coalescence process, whereas P2 was vertically diffused towards P3 (largest germ). Therefore, while the sizes of P1 and P2 were decreasing, the P3 size was increasing (see Figure S6a of supplementary materials). The diffusion process became extremely fast at frame 3, leading to an avalanche process where the whole particle was absorbed only in one frame. This could be clearly seen in the growth video (movie S4). We observed that the VD process was intensified by the increase of the overlap area between the particles. An analysis of the variation of the particle area as well as the overlap ratio between the germs, as a function of time step, for four different VD events is presented in Figure S6b-S6e of the supplementary materials. The VD process was observed at all investigated temperatures (350, 400 and 600 °C). For instance, the analysis of another event of VD process is presented in Figure S7 and movie S5 of the supplementary materials.

The vertical exchange between the two faces of the S-SLG is schematically illustrated in Figure 4d. For the VD process to occur, the atom of the germ face 1 (F1) must go through, at least, two energy barriers, schematically represented in Figure 4e. These barriers include

the bond breaking between the atom and its neighbors from the germ in face 1 (1) and the crossing of the graphene layer (2). We believe that any conditions allowing the reduction of one or more barriers will increase the exchange probability.

For the vertical atomic exchange to take place from one side to another side, at least one of the following conditions must be fulfilled:

(1) Overlap of the germs by their peripheries i.e. the periphery of the germ on face 1 (face 2) with the presence of a germ on the other face.

(2) A defect in the graphene layer (voids, missing atoms, grain boundaries, dangling bonds…). The presence of a defect in the graphene layer could significantly decrease the energy barrier preventing the diffusion of molecules through it.

Following these two points, we believe that the vertical atomic diffusion through the S-SLG can take place if only there was a stable germ on each side of the graphene layer. This was confirmed by the experimental data, as we did not observe a single germ diffusing spontaneously from one side to another, without the presence of a stable germ on the opposite side of the graphene layer. This is because in the latter case the barrier should be high enough to prevent the VD, especially if the diffusing germ must create a new nucleus after the process. Therefore, the atomic exchange always takes place at the overlap between the germs.

Due to the evolution of the germs, one of the aforementioned situations occurs. As in the case of the direct ripening process (movie S2), the mechanism is very fast and abrupt. It seems analogous to opening a canal between the planes and suddenly the process occurs. However, when the germs grow on both sides of the S-SLG and their mutual overlap grows (see Figs. S6b-S6e of the supplementary materials), the covered graphene surface area changes as well. This means that, with enough time, the peripheries of the two germs can be connected, generally at two points (Figure S7c of the supplementary materials), which favor the exchange between the germs, through graphene, and it occurs instantaneously.

The previous observations show that the remote interactions of Ge germs through the S-SLG play an important role in the observed process of atomic diffusion through graphene (Figure 4b, movies S4 and S5). In fact, graphene transparency towards the chemical interactions has been proven by observing that the wetting angle of water droplets on graphene depends on the underlying substrate. This, additionally, shows that substrate properties including atomic arrangement are able to penetrate one or few graphene layers.[34] Therefore, the “lattice transparency” of graphene enables remote interatomic interactions,

which were recently demonstrated during the remote epitaxy of different materials.[14],[15] In the remote epitaxy, which is governed by the atomic interactions, the graphene layer is sufficiently thin and electrically penetrable, to guide the epitaxial orientation of over-layers. Our experimental data present a clear evidence of these remote atomic interactions in real time, which are found to be very strong (see Figure S8 and movies S4, and S6 of the supplementary materials). Such interatomic interactions are most likely one of the main causes of the VD through the single layer graphene. In addition, through the growth videos, we observed that VD do not occur when germ peripheries are not in touch, despite a total overlap between them (see Figure S8b and movie S6 of the supplementary materials). This is a further evidence showing that during the VD through graphene, the involved germs should be overlapped by their peripheries. Moreover, the VD could also be explained by the permeability of graphene layers to atoms and molecules under specific conditions.[35],[36],[37],[38]

Taken together, our observations highly suggest that the VD through the S-SLG is due to the strong remote interatomic interactions induced by the formation of heterostructures (Ge/S-SLG/Ge i.e. 2D/2D/2D). The hexagonal ring of the graphene layer, which presents a geometric pore of 0.064 nm, expands when an atom passes through it. *Tsetseris et al.*[38] reported similar observations in the case of boron atoms passing through an SLG upon a mild annealing condition. In addition, our experimental lend support to the argument that the vertical exchange probability of Ge atoms between the 2 sides of the graphene layer is enhanced when the overlap ratio increases. However, even with a total overlap between Ge germs, that probability is very low in the cases where surface atoms are involved. Based on all the observations, the vertical exchange could be explained as a dynamic effect. Once there is an event triggering the diffusion process between the two faces, it produces a perturbation in the graphene layer, which decreases the penetration energy barrier and open a canal between the two planes. This led to a chaotic effect, where all the atoms are suddenly transferred from one side to another. As previously mentioned, another aspect allowing diffusion through a graphene layer is the presence of defects including vacancies and GB. However, even though we did not directly observe defects in the S-SLG (Figure S9 of the supplementary materials, attesting the high-quality of graphene layers), the high-voltage electron beam could induce defects such as vacancies and nanopores in the SLG. Other factors influencing the vertical exchange of Ge atoms though the SLG are summarized in the table S2 of the supplementary materials.

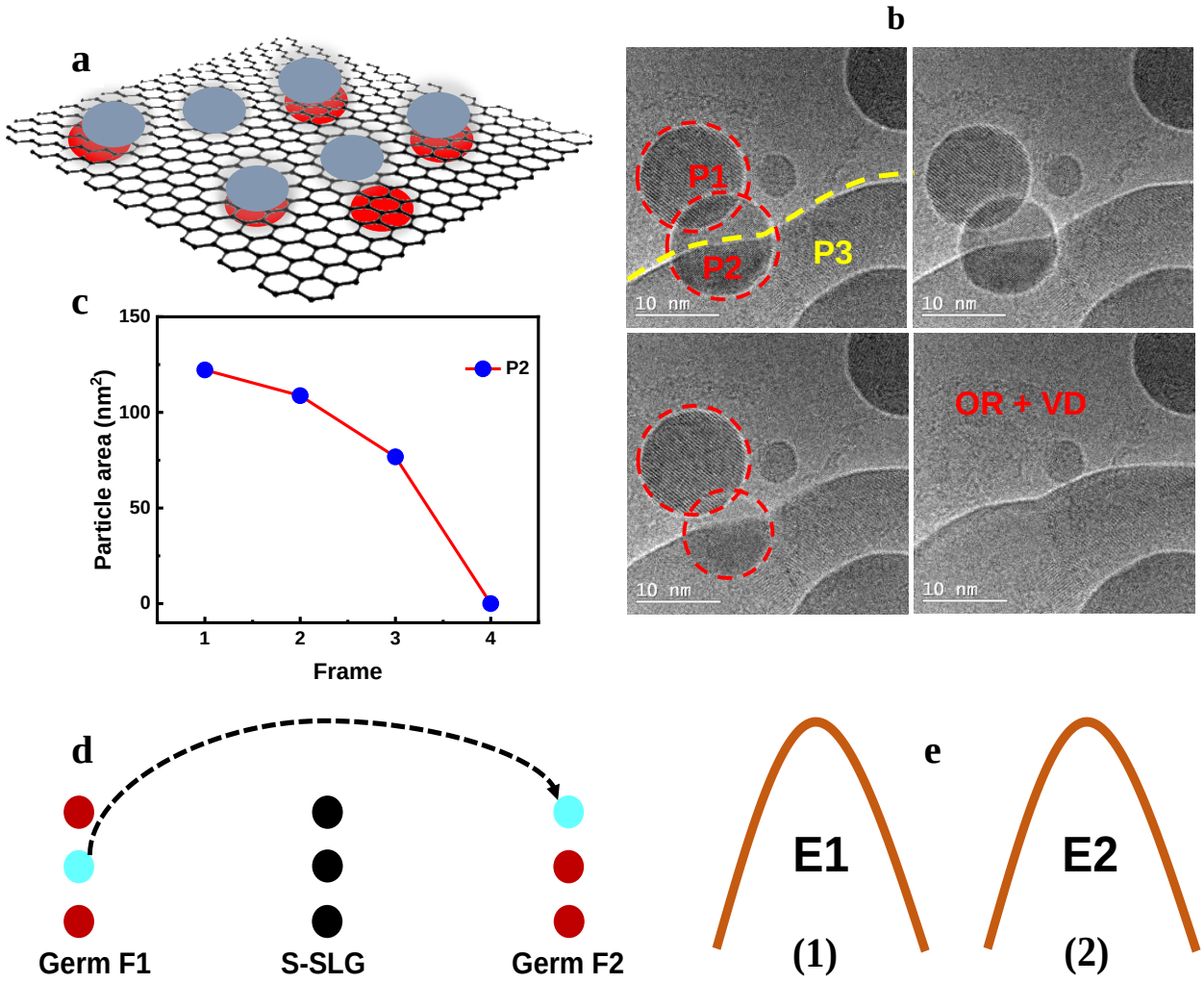

Figure 4. In-situ TEM observation of Ge/S-SLG/Ge heterostructures growth by UHV-CVD. (a) Schematic illustration displaying Ge crystals growing on both sides of a suspended single layer graphene. (b) Sequence of HRTEM images (with 0.25s intervals) illustrating a vertical diffusion (VD) (exchange) of Ge nanostructures through the single graphene layer at Tg= 400 °C. P1 and P3 are Ge particles located on the same side, whereas P2 is located on the opposite side. (c) plot of the particle area decreasing, for P2, during the VD as a function of frames. Each frame is 0.25s. (d) schematic illustration showing the diffusion of a Ge atom through the S-SLG from one side (F1) to another side (F2) and its bonding processes. (e) schematic illustration displaying the different energy barriers during the VD from one side to another side, through the S-SLG: (1) Bond breaking between the atom and its neighbors from the germ face 1, (2) Crossing of the graphene layer. E1 and E2 are the energies involved in the different steps.

3. Conclusions

In summary, we observed in real-time the nucleation and the growth of Ge on suspended single layer graphene using an in situ TEM system. Due to the low surface energy of the graphene layer, the nucleation was found to be very challenging on pristine and defect-free graphene layers. To enhance the nucleation on the clean graphene surface, a two-step nucleation strategy was used: nucleating at low temperature (220 °C) and annealing at higher

temperatures, for obtaining a better crystalline quality. Through the HRTEM growth videos, the critical size enabling the nucleation was experimentally determined. Moreover, the real-time observation of the growth provided a clear evidence that the Ge germs are almost floating at the top of the underlying graphene substrate making the diffusion extremely fast due to weak VdW interactions between them.

Growth mechanism of Ge on S-SLG was also established. Our experimental data demonstrated that the coarsening process is dominated by Ostwald ripening controlled by the rate of attachment-detachment process at the germ's boundaries. In addition, our investigations provided insights into the crystalline structure and the epitaxial relationship. The Ge crystals have a diamond cubic (DC) structure with two epitaxial relationships at low and high temperatures.

Notably, using freestanding graphene layers and UHV-CVD technique allowed the development of Ge/S-SLG/Ge (2D/2D/2D) heterostructures. The growth videos showed that in these double heterostructures, there is a vertical diffusion of Ge particles through the SLG. This is attributed to strong remote interatomic interactions through the SLG, which trigger a vertical transport of the atoms through the graphene lattice. These impressive and intriguing observations, which are not directly accessible via conventional ex situ analyses after the growth, are major findings in the understanding of the interactions between the epilayer (3D semiconductor) and the underlying graphene layer. Moreover, the 2D/2D/2D heterostructures can offer a great opportunity for a whole new physics that is yet to come, such as superconductivity and quantum wells.

Overall, we have demonstrated that in-situ TEM allows the real-time observation of the growth of Ge on S-SLG and offers great potential for bringing new interpretations into crystal growth and addressing many raised fundamental questions in materials science. Therefore, we believe that these new insights not only will be a great impact on the understanding of VdWE mechanisms of semiconductors on graphene, but also, they will provide a new pathway for disruptive hybrid devices in which a reliable and successful nucleation must be controlled.

4. Materials and Methods

Substrate preparation

A fusion thermal E-chips supplied by Protochips was used as a substrate for the in situ experiments. It consists of a central heating SiC membrane supported by a silicon substrate, with nine holes, arranged in a 3x3 array, each 8µm in diameter and separated by 12µm

(Figure S1a of the supplementary materials). These holes are located in the center of the membrane to provide an electron transparent area for transmission electron microscopy imaging. The heating of the central membrane of the chips is ensured by Joule effect provided by the sample holder (see Figure S1b of the supplementary materials), which enables high thermal stability (<0.1 °C/min), a uniform heating, and a small sample displacement. Suspended single layer graphene (S-SLG) were obtained by transferring graphene on the central membrane of the E-chips. This step was carefully performed since the quality of graphene layers is crucial for the in situ nucleation and growth observation.

Before graphene transfer, a thin oxide layer was deposited on the E-chips to prevent short circuit because the graphene layers are good electrical conductors. For this purpose, a few nanometers (about 10 nm) of aluminum oxide (Al_2O_3) was deposited on the chips (see Figure S1c of the supplementary materials) by using atomic layer deposition (ALD). However, even in that configuration, the graphene layers should be transferred in a way that they do not entirely cover the contacts of the chips. Note that the oxide deposition did not affect the chip resistance or the graphene transfer.

After the oxide layer deposition, graphene layer transfer was performed. Easy transfer monolayer graphene (1ML) ordered from Graphenea were used in that step. An easy transfer graphene consists of a 1ML graphene supported by a polymer and capped by a sacrificial layer (PMMA). The stack PMMA/SLG is weakly bonded to the polymer support and thus easily detachable from it. The graphene transfer is proceeded in three steps (see Figure S2a of the supplementary materials):

- Release from the polymer support: this step is performed by deionized water (DIW). We slowly put the sample in DIW while the sacrificial layer PMMA/SLG is detached from the polymer support. Once the PMMA/SLG is floating, we remove the polymer film.
- Transfer: here the floating PMMA/SLG layer is deposited on the desired substrate. It is very useful that the host substrate has a hydrophilic surface. For this reason, to have a hydrophilic surface, the chips were treated by an oxygen plasma for 5 min (150 W, 330 mTorr). We introduce the host substrate into the DIW, and we carefully fish the PMMA/SLG layer from below. Once the layer is deposited on the substrate, we let it dry for 30 min in ambient air (clean rooms). Then we anneal the sample on a hot plate at 150 °C for 1h. finally, before the removal of the PMMA sacrificial, to avoid the detachment of the graphene from the chips, the sample is stored under vacuum for 24h.
- PMMA removal: the PMMA was dissolved by using the solvent method (acetone and isopropyl alcohol, IPA). To reduce the surface tension of acetone and to efficiently remove

the PMMA, the acetone solution was heated at 50 °C during the process. To prevent the break of the suspended graphene layer, the sample was not entirely dipped in the solution but rather it was placed in the way only the surface was touched by the acetone solution. After 15 min of cleaning in the hot acetone, the sample was rinsed in IPA for 5 min to remove the rest of acetone. SEM image and a Raman spectrum of a S-SLG are presented in Figure S2b and Figure S2c, respectively. After the solvent method cleaning and before the growth, the samples were loaded into the ultra-high vacuum (UHV) TEM chamber and annealed at 600 °C for 1.5h to remove polymer residues remaining from the process. It is worth mentioning that the PMMA dissolution is a crucial step, therefore should be carefully performed to obtain very clean graphene layers. In fact, as shown by the Figure S2d, any deviation from the perfect cleaning will result in PMMA residues and defects, which could act as preferential nucleation sites preventing the nucleation on the clean regions of the graphene layers. The nucleation on such residues leads to a polycrystalline growth as shown by the Figure S2e. This is a further evidence showing that one of the major limitations of the in-situ growth on graphene is the cleaning processes of the layers prior to the growth.

In situ growth

Direct in situ observations of nucleation and growth were carried out in a Cs-corrected Titan environmental TEM (Titan 60-300 ETEM), equipped with gaseous sources for UHV chemical vapor deposition (UHV-CVD) and custom-made molecular beam epitaxy sources. During the in situ experiments, the ETEM was operated at 300 kV. For Ge growth, 10% diluted digermane (Ge_2H_6 + 90% H_2) was used as a precursor. A flow of 0.2 sccm was used for all the experiments. The growth of Ge on S-SLG was performed at different growth temperatures (Tg) ranging from 220 to 600 °C. the nucleation on the clean graphene was obtained at low temperature (220°C). However, at such low temperature the crystalline quality of the Ge germs is very low and, thus the nucleation process is followed by an annealing step at higher temperature. High-resolution movies were recorded using a Gatan US1000 camera at a rate of 4 frames per second. Images and movies were analyzed using Image J and Gatan GMS software. The growth kinetics were determined from the growth videos by extracting particle areas, density of visible germs and diffraction patterns.

Additional characterizations were performed on the S-SLG using Raman spectroscopy and scanning electron microscopy (SEM). Raman measurements were carried out using a Renishaw spectrometer equipped with a CCD detector and a laser with an excitation wavelength of 532 nm. The SEM imaging was carried out using a Zeiss Leo III, operating from 1 kV to 20 kV and equipped with a field emission gun.

Supplementary Materials
Supporting Information is available from the Wiley Online Library and contains:
Supplementary text
Figures S1 to S7
Tables S1 to S2
Movies S1 to S6

5. Acknowledgements

The authors would like to thank H. Pelletier, G. Bertrand, and P.O. Provost for the technical help, Javier Arias Zapata for scientific discussions and graphene transfer process, Ahmed Ayari for sample preparation, Federico Panciera and the material department at C2N center for their assistance with in situ TEM experiments, Ileana Florea, and Laurent Travers for technical assistance. We acknowledge the Natural Sciences and Engineering Research Council of Canada (NSERC), MITACS, the Arbor Foundation and the Fonds de Recherche du Quebec-Nature et Technologies (FRQNT) for financial support.
Authors declare no competing interests.

Received: ((will be filled in by the editorial staff))
Revised: ((will be filled in by the editorial staff))
Published online: ((will be filled in by the editorial staff))

References

[1] S. H. Bae, H. Kum, W. Kong, Y. Kim, C. Choi, B. Lee, P. Lin, Y. Park, J. Kim, Nat. Mater. 2019, 18, 550.

[2] D. Ruzmetov, K. Zhang, G. Stan, B. Kalanyan, G. R. Bhimanapati, S. M. Eichfeld, R. A. Burke, P. B. Shah, T. P. O'regan, F. J. Crowne, A. G. Birdwell, J. A. Robinson, A. V Davydov, T. G. Ivanov, ACS Nano 2016, 10, 3580.

[3] L. Britnell, R. V. Gorbachev, R. Jalil, B. D. Belle, F. Schedin, A. Mishchenko, T. Georgiou, M. I. Katsnelson, L. Eaves, S. V. Morozov, N. M. R. Peres, J. Leist, A. K. Geim, K. S. Novoselov, L. A. Ponomarenko, Science (80-.). 2012, 335, 947.

[4] W. J. Yu, Z. Li, H. Zhou, Y. Chen, Y. Wang, Y. Huang, X. Duan, Nat. Mater. 2013, 12, 246.

[5] H. Yang, J. Heo, S. Park, H. J. Song, D. H. Seo, K. E. Byun, P. Kim, I. K. Yoo, H. J. Chung, K. Kim, Science (80-.). 2012, 336, 1140.

[6] K. Chung, C.-H. Lee, G.-C. Yi, Science (80-.). 2010, 330, 655.

[7] C. H. Liu, Y. C. Chang, T. B. Norris, Z. Zhong, Nat. Nanotechnol. 2014, 9.

[8] N. Nerngchamnong, L. Yuan, D. C. Qi, J. Li, D. Thompson, C. A. Nijhuis, Nat. Nanotechnol. 2013, 8, 113.

[9] Y. J. Hong, J. W. Yang, W. H. Lee, R. S. Ruoff, K. S. Kim, T. Fukui, Adv. Mater. 2013, 25, 6847.

[10] Y. Wang, J. C. Kim, R. J. Wu, J. Martinez, X. Song, J. Yang, F. Zhao, A. Mkhoyan, H. Y. Jeong, M. Chhowalla, Nature 2019, 568, 70.

[11] Y. Alaskar, S. Arafin, D. Wickramaratne, M. A. Zurbuchen, L. He, J. McKay, Q. Lin, M. S. Goorsky, R. K. Lake, K. L. Wang, Adv. Funct. Mater. 2014, 24, 6629.

[12] S. Mukherjee, N. Nateghi, R. M. Jacobberger, E. Bouthillier, M. de la Mata, J. Arbiol, T. Coenen, D. Cardinal, P. Levesque, P. Desjardins, R. Martel, M. S. Arnold, O. Moutanabbir, Adv. Funct. Mater. 2018, 28.

[13] P. Periwal, J. D. Thomsen, K. Reidy, G. Varnavides, D. N. Zakharov, L. Gignac, M. C. Reuter, T. J. Booth, S. Hofmann, F. M. Ross, Appl. Phys. Rev. 2020, 7.

[14] Y. Kim, S. S. Cruz, K. Lee, B. O. Alawode, C. Choi, Y. Song, J. M. Johnson, C. Heidelberger, W. Kong, S. Choi, K. Qiao, I. Almansouri, E. A. Fitzgerald, J. Kong, A. M. Kolpak, J. Hwang, J. Kim, Nature 2017, 544, 340.

[15] W. Kong, H. Li, K. Qiao, Y. Kim, K. Lee, Y. Nie, D. Lee, T. Osadchy, R. J. Molnar, D. K. Gaskill, R. L. Myers-Ward, K. M. Daniels, Y. Zhang, S. Sundram, Y. Yu, S. hoon Bae, S. Rajan, Y. Shao-Horn, K. Cho, A. Ougazzaden, J. C. Grossman, J. Kim, Nat. Mater. 2018, 17, 999.

[16] S. H. Bae, K. Lu, Y. Han, S. Kim, K. Qiao, C. Choi, Y. Nie, H. Kim, H. S. Kum, P. Chen, W. Kong, B. S. Kang, C. Kim, J. Lee, Y. Baek, J. Shim, J. Park, M. Joo, D. A. Muller, K. Lee, J. Kim, Nat. Nanotechnol. 2020, 15, 272.

[17] B. J. Kim, J. Tersoff, S. Kodambaka, M. C. Reuter, E. A. Stach, F. M. Ross, Science (80-.). 2008, 322, 1070.

[18] S. Sauze, M. R. Aziziyan, P. Brault, G. Kolhatkar, A. Ruediger, A. Korinek, D. Machon, R. Arès, A. Boucherif, Nanoscale 2020.

[19] N. T. K. Thanh, N. Maclean, S. Mahiddine, Chem. Rev. 2014, 114, 7610.

[20] D. R. Cassar, J. Non. Cryst. Solids 2019, 511, 183.

[21] E. Cahyadi, Adsorption of Carbon, Silicon, and Germanium Adatoms on Graphene Sheet, UNIVERSITY OF CALIFORNIA Los Angeles, UCLA, 2012.

[22] V. N. E. Robinson, J. L. Robins, Thin Solid Films 1974, 20, 155.

[23] P. Sutter, E. Sutter, ACS Appl. Nano Mater. 2018, 1, 3026.

[24] H. Zheng, R. K. Smith, Y. W. Jun, C. Kisielowski, U. Dahmen, A. Paul Alivisatos, Science (80-.). 2009, 324, 1309.

[25] J. Zhang, F. Huang, Z. Lin, Nanoscale 2010, 2, 18.

[26] H. O. K. Kirchner, Metall. Trans. 1971, 2, 2861.

[27] N. Bartelt, W. Theis, R. Tromp, Phys. Rev. B - Condens. Matter Mater. Phys. 1996, 54, 11741.

[28] F. Haußer, A. Voigt, Phys. Rev. B - Condens. Matter Mater. Phys. 2005, 72, 1.

[29] F. Huang, H. Zhang, J. F. Banfieldt, Nano Lett. 2003, 3, 373.

[30] A. M. Munshi, D. L. Dheeraj, V. T. Fauske, D. C. Kim, A. T. J. Van Helvoort, B. O. Fimland, H. Weman, Nano Lett. 2012, 12, 4570.

[31] Z. Lu, X. Sun, W. Xie, A. Littlejohn, G. C. Wang, S. Zhang, M. A. Washington, T. M. Lu, Nanotechnology 2018, 29.

[32] H. Gao, J. Zhou, M. Lu, W. Fa, Y. Chen, J. Appl. Phys. 2010, 107.

[33] Kengo Nakada and Akira Ishii, InTech, 2011, p. 376.

[34] S. Chae, S. Jang, W. J. Choi, Y. S. Kim, H. Chang, T. Il Lee, J. O. Lee, Nano Lett. 2017, 17, 1711.

[35] M. Lozada-Hidalgo, S. Hu, O. Marshall, A. Mishchenko, A. N. Grigorenko, R. A. W. Dryfe, B. Radha, I. V. Grigorieva, A. K. Geim, Science (80-.). 2016, 351, 68.

[36] P. Z. Sun, Q. Yang, W. J. Kuang, Y. V. Stebunov, W. Q. Xiong, J. Yu, R. R. Nair, M. I. Katsnelson, S. J. Yuan, I. V. Grigorieva, M. Lozada-Hidalgo, F. C. Wang, A. K. Geim, Nature 2020, 579, 229.

[37] E. Griffin, L. Mogg, G. P. Hao, G. P. Hao, G. Kalon, G. Kalon, C. Bacaksiz, G. Lopez-Polin, G. Lopez-Polin, T. Y. Zhou, V. Guarochico, J. Cai, C. Neumann, A. Winter, M. Mohn, J. H. Lee, J. Lin, J. Lin, U. Kaiser, I. V. Grigorieva, K. Suenaga, B. Özyilmaz, H. M. Cheng, H. M. Cheng, W. Ren, A. Turchanin, F. M. Peeters, A. K. Geim, M. Lozada-Hidalgo, ACS Nano 2020, 14, 7280.

[38] L. Tsetseris, S. T. Pantelides, Carbon N. Y. 2014, 67, 58.